International Journal of Multidisciplinary Engineering in Current Research
Volume 6, Issue 9, September 2021, http://ijmec.com/

MEDICAL IMAGE FUSION BASED ON FEATURE EXTRACTION AND SPARSE REPRESENTATION

DR.Mohammad Sanaullah Qaseem[1], Mohd Khaleel Ahmed[2]
Professor[1], Asst.Prof[2]
Department of cse
NAWAB SHAH ALAM KHAN COLLEGE OF ENGINEERING & TECHNOLOGY
NEW MALAKPET, HYDERABAD-500024

Abstract

Sparse representation has numerous benefits over traditional picture representation approaches as a novel multiscale geometric analysis technique. The normal sparse representation, on the other hand, ignores inherent structure and time complexity. A new fusion mechanism for multimodal medical images focused on sparse representation and judgment is presented in this article.

A map is planned to address both of these issues at the same time. To allow the effects reserve more energy and edge knowledge, three decision maps are designed: structure information map (SM), energy information map (EM), and structure and energy map (SEM). The Laplacian of a Gaussian (LOG) captures the local structure function in SM, and the mean square variance detects the energy and energy distribution feature in EM. To increase the pace of the algorithm, the decision map is applied to the standard sparse representation dependent procedure. By improving the contrast and reserving more structure and energy details from the source pictures, the proposed solution also enhances the accuracy of the fused data. The findings of 36 classes of CT/MR, MR-T1/MR-T2, and CT/PET photos show that the SR and SEM-based approach outperforms five state-of-the-art approaches.

1. INTRODUCTION

Thanks to the growing demands of clinic inquiry and disease diagnosis, medical imaging is gaining in popularity. Medical imaging is complicated by a variety of imaging processes.In a small domain, photographs of various modals include a variety of complementary details regarding the human body.

For eg, computed tomography (CT) images provide better information on thick tissue, PET images provide better information on blood flow and tumor activity with low spatial resolution, and magnetic resonance (MR) images provide better information on soft tissue. Furthermore, MR-T1 images provide more information regarding anatomical shapes, while MR-T2 images provide a stronger distinction between regular and abnormal tissues. However, a single multiple modalities would not be able to meet the need for high-resolution imagery and simulation for disease diagnosis.Medical picture fusion is a valuable and efficient strategy for combining complementary details from multimodality images to increase diagnostic precision in this regard.

Furthermore, fused images are better for assisting doctors in diagnosis and care preparation : fusing MR and CT images will provide images that describe soft tissue and bone while simultaneously representing anatomical and physiological aspects of the human body. To segment white matter lesions and direct neurosurgical resection of epileptogenic lesions, MR-T1 and MR-T2 photos are fused . In oncology, hybrid PET/CT imaging is useful for viewing biological, biochemical, and tumor response characteristics. Furthermore, medical picture fusion not only aids in disease diagnosis but also lowers storage.Multistage decomposition approaches have grown in popularity as the most widely used image fusion process.

Discrete wavelet transform (DWT), frame let transform contour let transform and nonsubsampledcontour let transform (NSCT) have all been established in recent years. Regrettably,In the presence of noise, transform-based approaches yield low fusion effects, and choosing the decomposition levels is challenging.Since sparse representation (SR) has proved to be an extremely useful method for

International Journal of Multidisciplinary Engineering in Current Research
Volume 6, Issue 9, September 2021, http://ijmec.com/

processing high-dimensional signals more and more researchers are applying it to the field of picture fusion to improve fused outcomes .

The regular SR, on the other hand, ignores the intrinsic structure and the time complexity. As a result, incorporating them into the SR model is a rational approach for improving SR but determining the connection between intrinsic structure knowledge and sparse coefficients is difficult. Reference suggested a dictionary learning approach that combined geometrical structure with group sparse coding, but it did not discuss the time complexity of the sparse representation algorithms. Picture fusion approaches focused on joint sparse representation (JSR) and need a significantly higher number of iterations to achieve image vector sparse representation for a larger qualified vocabulary. Some researchers suggested new methods combining multistage transform and SR to fuse the source images' structure details into the fused images, but these methods are far more complicated and time consuming.

As a result, the main challenge became how to achieve picture fusion dependent on SR with local structure knowledge in less time. By extracting the local structure function of the picture blocks, the decision map will assist us in achieving this aim. Unfortunately, the majority of judgment map-based approaches are only suitable for multifocal picture fusion. The decision map is used in infrared and visible picture fusion in references demonstrating that it can be used for other types of image fusion. In particular, almost all sparse coefficients fusion rules for SR methods are dependent on different blocks feature values, implying that they are all decision map methods . We incorporate the local structure and energy details of source images into the decision map to increase the pace of the algorithm and the accuracy of the fused effects in order to realize medical image fusion based on SR with decision map.

This paper's main contribution is as follows:

(1) To incorporate the source images' local structure and energy details into the SR algorithm for medical image fusion, we generated three decision maps to remove the source images' local energy and structure features.

(2) It is beneficial to use the decision to reduce the amount of picture blocks to coarse representation in order to obtain faster performance. The accuracy of the findings would also increase if the maps are used to keep more structure and energy details in fused pictures.

2. The Proposed Method's Framework

Figure 1 show the architecture of the suggested solution, which is focused on SR and function extraction.To begin, we divide all source images into two groups, A and B, based on their scale.$m\times n$ into patches yi, 1and $yi,j2$ through a sliding window withthe size of$\times w(i \le m-w,\ j \le n-w)$. All patches are arrangedinto vectors $(i-1)*(n-w)+j1$ and $V(i-1)*(n-w)+j2$ from left to rightand from top to bottom.Second, we divide these vectors into vector pairs based on the initial patches' corresponding locations, and construct the decision map for each pair separately.

Finally, when the map is labeled as 1 or 2, we use the decision map to decide whether one vector in each category is the product. When the map is labeled 0, it implies that these classes are known as the sparse representation system's input.
Finally, we use the SRmethod to fuse the remaining vector pairs.Finally, based on the judgment diagram, the machine may produce fused data. The patches' overlaps are averaged.SR. 2.1. A signal can be expressed in SR algorithms as a sparse mixture of the fewest possible atoms from an over complete dictionary.
Let VRmdenote a signal vector from the source images and let $m\times k(k>m)$ denote an over complete dictionary whose column vectors are its atoms. The signal vector can be represented as$V = D\theta$, whereis a sparse coefficient vector. The sparse o efficient vector is acquired by solving the following question:

International Journal of Multidisciplinary Engineering in Current Research
Volume 6, Issue 9, September 2021, http://ijmec.com/

$$\hat{\theta} = \arg\min_{\theta} \quad \|\theta\|_0 \qquad (1)$$
$$\text{s.t.} \quad \|V - D\theta\|_2^2 \le \varepsilon,$$

Where is the parameter for error tolerance? A superposition of the smallest number of atoms in the dictionary can be used to describe a picture vector. (1) Can be solved bysince it is an NP-hard challenge, use OMP, BP, or other algorithms. It is critical to locate a suitable dictionary for SR. There are two major methods for creating a dictionary. The Gabor dictionary], the discrete cosine transform (DCT) and the Haar dictionary are examples of set dictionaries. Another choice is to use K-SVDto train a dictionary from a large number of training image patches, which normally outperforms fixed dictionary methods in image processing.

2.2. The EnergyMap and the StructureMap.

Let us regard yi, 1 and yi, 2 as mean values of yi,1 and yi, 2 , respectively.We use $\|yi,j\ 1\ \|2$ as the sign of energy and the mean square deviation$(1/64)\|yi,j1 - yi,j1\ \|2$ as the sign of energy distribution for $yi,j1$,which are similar to $yi,j2$. We design the first decision mapEM $\in RM\times N$(where$M = m-$ wand $N = n - w$) whichcalled the energy map by

$$t1 = \frac{1}{64}\left(\left\|y_1^{i,j}\right\|_2 - \left\|y_2^{i,j}\right\|_2\right),$$

$$t2 = \frac{1}{64}\left(\left\|y_1^{i,j} - \overline{y}_1^{i,j}\right\|_2 - \left\|y_2^{i,j} - \overline{y}_2^{i,j}\right\|_2\right),$$

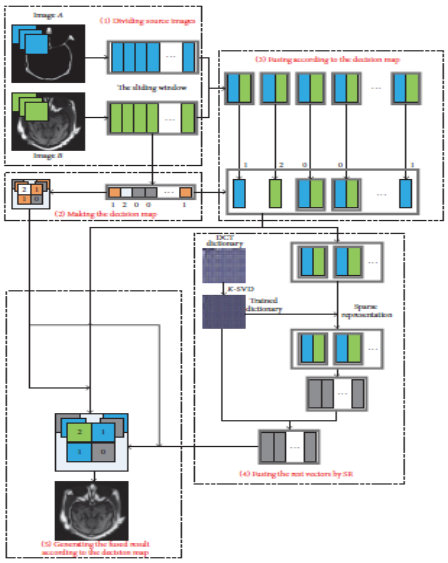

Figure 1: The framework of the image fusion method based on sparse representation and feature extraction.

$$EM^{i,j} = \begin{cases} 1, & t1 > 0,\ t2 > 0, \\ 2, & t1 < 0,\ t2 < 0, \\ 0, & \text{others.} \end{cases} \qquad (2)$$

As a result, ourmap provides details about the space and energy distribution of the vector pairs. This chart, however, lacks sufficient image structure detail. To detect the structure details of the source pictures, the Laplacian of a Gaussian (LOG) was used We smooth the picture for noise reduction by convolving it with a digital mask that corresponds to the Gaussian function. (3)– (5) expresses the Gaussian function, and (3)–(5) expresses the local normalized structure details (6). There is more.

International Journal of Multidisciplinary Engineering in Current Research
Volume 6, Issue 9, September 2021, http://ijmec.com/

$$h(x,y) = h(r) = -e^{-r^2/2\sigma^2}, \quad (3)$$

$$\nabla^2 (g(r) * h(r)) = g(r) * \nabla^2 h(r), \quad (4)$$

$$p = g(r) * \nabla^2 h(r) = -g(r)\left[\frac{r^2-\sigma^2}{\sigma^4}\right] e^{-r^2/2\sigma^2}, \quad (5)$$

$$e = \frac{p}{\max(p)}, \quad (6)$$

Where$r2 = x2 + y2$ and $\sigma$is the mean square deviation. Given an image matrix (x, y), the LOG of the image function is the second-order partial derivatives along $x$and $y$directions. There is an example of the LOG edge detection of CT and MR images as shown in Figure 2. ei, 1 and ei,j 2 represent the local normalized structure information of yi,j 1 and yi,j 2 , respectively. Therefore, we design the second map SM $\times N$named the structure map by

$$s1 = \frac{1}{64}\left(\left\|e_1^{i,j}\right\|_2 - \left\|e_2^{i,j}\right\|_2\right),$$

$$s2 = \frac{1}{64}\left(\left\|e_1^{i,j} - \bar{e}_1^{i,j}\right\|_2 - \left\|e_2^{i,j} - \bar{e}_2^{i,j}\right\|_2\right), \quad (7)$$

$$SM^{i,j} = \begin{cases} 1, & s1 > 0.05,\ s2 > 0, \\ 2, & s1 < -0.05,\ s2 < 0, \\ 0, & \text{others.} \end{cases}$$

The Structure and Energy Map (2.3). We create the third map SEM RMN, which we call the system and combine the electricity, energy delivery, and structure detail energy map generated by

$$SEM^{i,j} = \begin{cases} 0, & EM^{i,j} = 0,\ SM^{i,j} = 0, \\ 1, & EM^{i,j} = 1, \\ 1, & EM^{i,j} = 0,\ SM^{i,j} = 1, \\ 2, & EM^{i,j} = 2, \\ 2, & EM^{i,j} = 0,\ SM^{i,j} = 2. \end{cases} \quad (8)$$

When $Vh\ 1 = D\theta h\ 1$ and $Vh\ 2 = D\theta h\ 2$, we can get the fusion vectors by (9) according to the decision map:

$$g\left(\theta_1^h, \theta_2^h\right) = \begin{cases} \theta_1^h, & \left|\theta_1^h\right| > \left|\theta_2^h\right|, \\ \theta_2^h, & \left|\theta_1^h\right| \le \left|\theta_2^h\right|, \end{cases}$$

$$F^h = \begin{cases} V_1^h, & M^{i,j} = 1, \\ V_2^h, & M^{i,j} = 2, \\ D \times g\left(\theta_1^h, \theta_2^h\right), & M^{i,j} = 0, \end{cases} \quad (9)$$

$$i = \left\lfloor \frac{h}{n-w} \right\rfloor,\ j = h - i * (n-w),$$

Where$M \times N$can be EM, SM, SEM, or other decision maps.In comparison to the traditional SR-based approach, the proposed method has at least three merits. For starters, it should ensure that the merged findings retain the source's content.

As far as practicable, exclude the influence of algorithm noise from the photographs. Second, since we just sparse-represent a portion of the vector pairs, we will get the results faster. Finally, our algorithm enhances contrast by combining energy, energy flow, and structure characteristics of the pictures. The proposed findings provide the strongest contrast details, which is the most relevant information for locating the location of the irregular tissue, according to the abstract.

3. Experiments

Experiments are carried out. The photos are all the same size, measuring 256 x 256 pixels. In this article, we use K-SV to train the dictionary. Duplicating the images in the manner seen in Figure 3. The blunderthe tolerance has been adjusted to 0.01.The K-cumulative SVD's iterations have been raised to 30. The first dictionary is the DCT dictionary, which has a scale of 64 256 characters. For convenience, we approximate the sparse coefficients with OMP. The sliding window's movement phase is set to one pixel.

International Journal of Multidisciplinary Engineering in Current Research
Volume 6, Issue 9, September 2021, http://ijmec.com/

To assess the accuracy of the abovementioned processes, we use three types of medical image pairs: CT/MR images, MR-T1/MRT2 images, and CT/PET images. Figure 4 depicts the DCT dictionary and the educated dictionary. LOG's window size is set to 5 and the number of columns is set to 2.

In the tests, five state-of-the-art methods are tested for reference, namely NSCT-based methods JSR-based methods and NSCT-based and SR-based methods To test the fusion efficiency in this article, five objective evaluation calculation parameters are used. Local quality index (Q0) weighted fusion quality index (QW) edge-dependent fusion quality index (QE) QAB/F all calculate the transmission of edge and visual knowledge from source images to fused images, while shared information (MI) computes the information transformed from source images to fused images. The interval is shared by Q0, QW, QE, and QAB/F. The higher the value for these parameters, the better the fusion results.

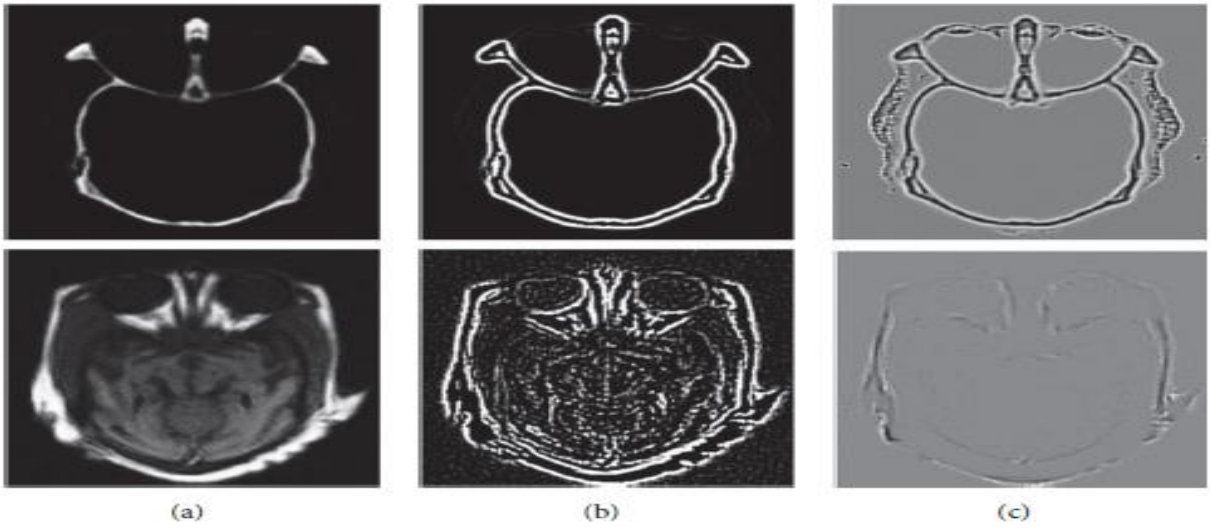

Figure 2: (a) The source images, (b) the structure information of LOG, and (c) the local structure information normalization.

International Journal of Multidisciplinary Engineering in Current Research
Volume 6, Issue 9, September 2021, http://ijmec.com/

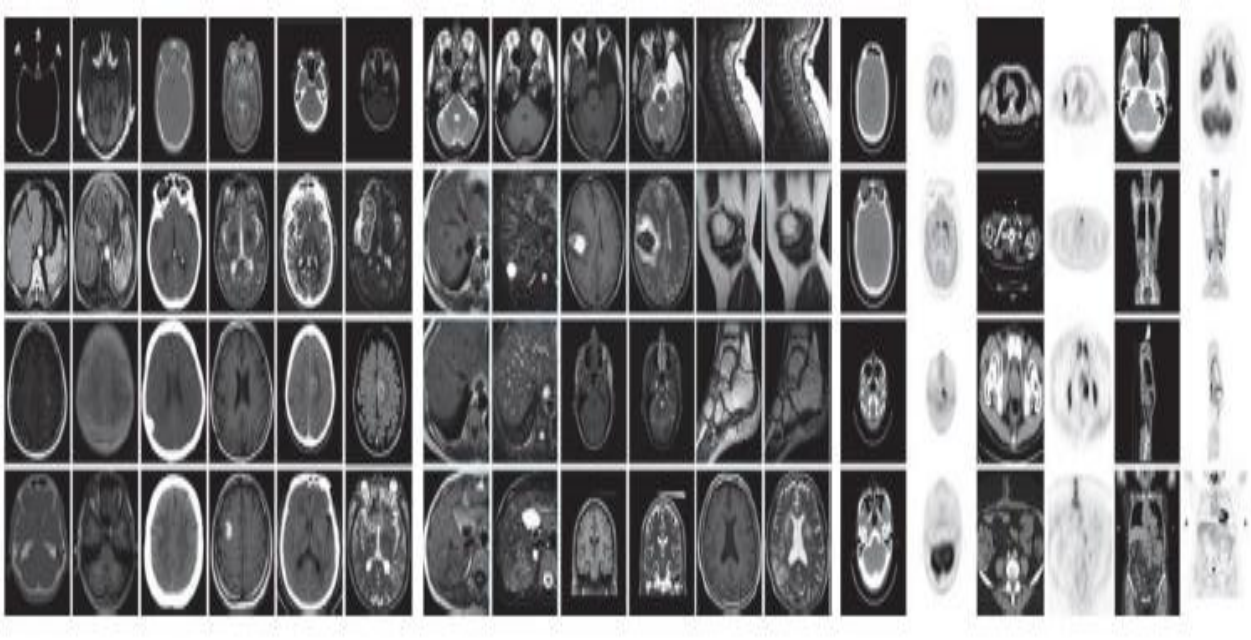

Figure 3: The source images for fusion and training dictionary, including 12 pairs of CT/MR images, 12 pairs of MR-T1/MR-T2 images, and 12 pairs of T/PET images.

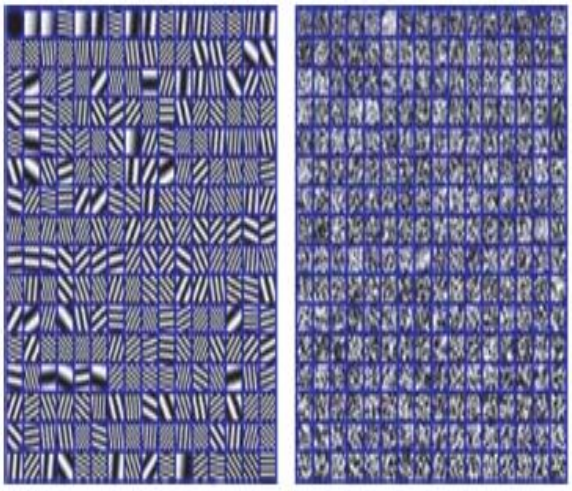

Figure 4: The DCT dictionary and the trained dictionary.

Experiments were run on a PC with an Intel i7-3770 CPU running at 3.40GHz and 4GB of RAM, running MATLAB R2010a.

3.1. Combination of CT and MR images.

The CT and MR images are fused in the first experiment using the eight image fusion methods mentioned above. As seen in Figure 3, we used 12 classes of CT and MR images to measure the accuracy of these approaches. Figure 5 depicts two sets of outcomes. The results of NSCT are clearly fuzzy in certain areas, especially in Figures 5(m) and 5(n), while the results of SR + NSCT SR + SM, and SR + SEM will reserve better source picture boundary knowledge than the results of the other methods. Since both of the strategies use the sliding window technique, NSCT and NSCT use a window with a size of 3 and the others use a window with a size of 8, these findings have no block consequences. And the NSCT NSCT JSR and SR + NSCT findings

International Journal of Multidisciplinary Engineering in Current Research
Volume 6, Issue 9, September 2021, http://ijmec.com/

are clearer than all source pictures, resulting in some dim detail being obscured by light information.
We can't say the tissue details between the skull and the cortex, as seen in Figures 5(m), 5(n), 5(o), and 5(q). To some point, the suggested approach should alleviate these issues while maintaining the benefits of SR-based approaches.
In comparison, the effects of SR + SEM will provide improved image boundary and energy information, allowing us to obtain better anatomical information from CT images while still obtaining soft tissue information from MR images.
Furthermore, in Figures 5(r), 5(s), and 5(t), the calcified meningioma in Figure 5(f) can be easily differentiated from the context (t). In terms of

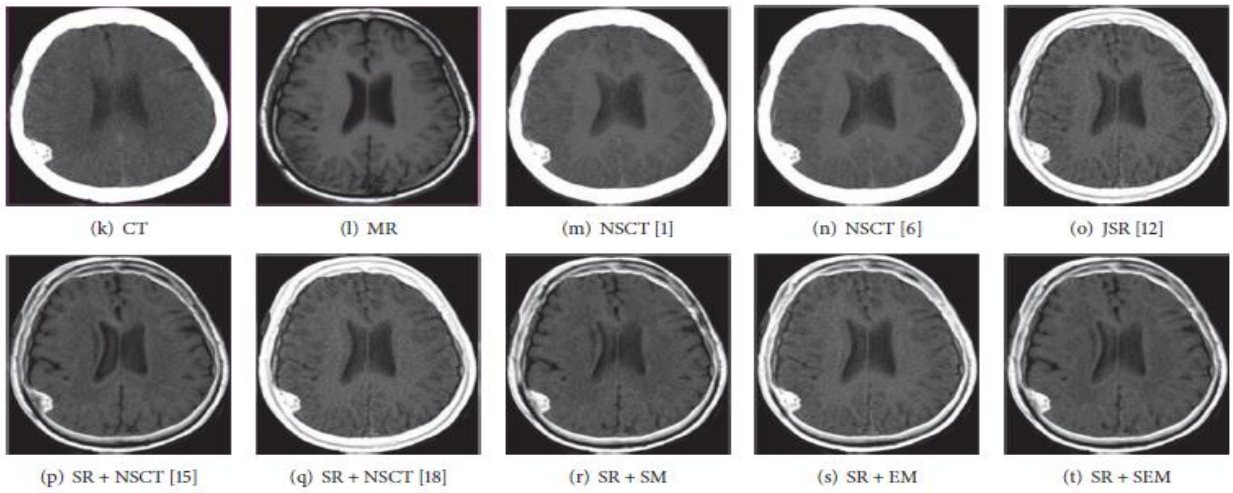

Figure 5: The CT and MR image fused results of different fusion methods.

Table 1 shows the combined CT and MR picture ratings, as well as the average scores of predictive measurement criteria, with the "bold" values indicating the maximum values. If we can tell, themethod suggested in any case, SR + SEM outperforms other approaches. The proposedmethods' combined findings are all superior to traditional approaches.
3.2. Image Fusion of MR-T1 and MR-T2. As seen in Figure 3, we used 12 classes of MR-T1 and MR-T2 photos to measure the accuracy of these methods in the second experiment.Figure 6 shows two sets of experiments to demonstrate the proposed fusion process. The effects of NSCT [1], NSCT [6], and SR + NSCT [18] are gloomy and vivid in general, showing grey distortion. Many bad edges are generated by NSCT [1], NSCT [6], JSR [12], and SR + NSCT [18], and the fused effects are too smooth. In comparison, the findings of SR + NSCT [15] and proposedmethods show improved boundary and energy details with less objects, allowing us to extract more information on adipose tissue from MR-T1 images and vascular and tumor information from MR-T2 images. The suggested methods' findings provide more detail from the source images than the other methods. The proposed methods retain better local edge and texture detail, all of which are critical for diagnosis. Figure 6(l) shows the subacute premature hematoma, and Figures 6(r), 6(s), and 6(t) show the direction and contour of the intracranial hematoma (t). Table 2 lists the average scores of quantitative evaluationmetrics for 12 MR-T1 and MR-T2 fused results, with the "bold" points indicating the highest ratings.

International Journal of Multidisciplinary Engineering in Current Research
Volume 6, Issue 9, September 2021, http://ijmec.com/

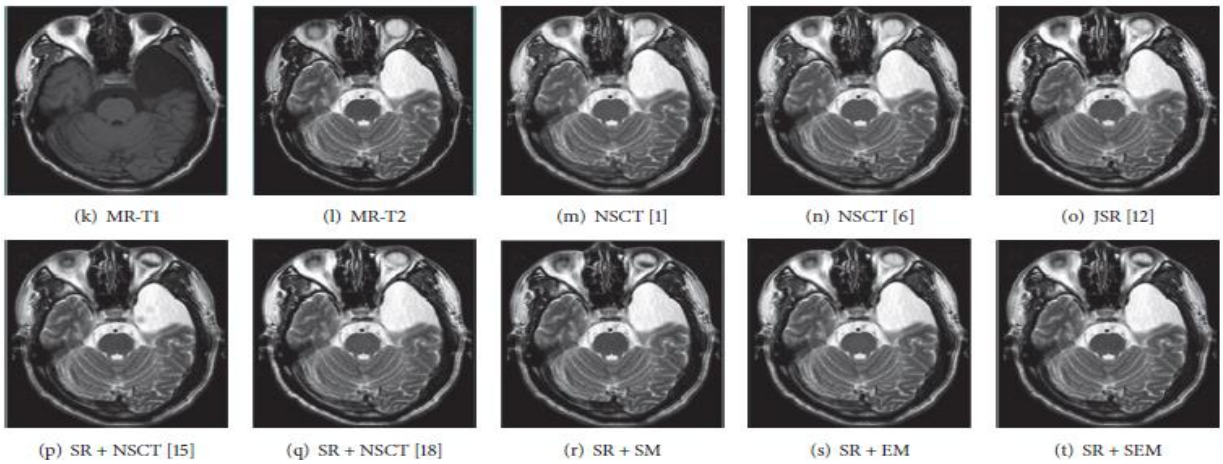

Figure 6: The MR-T1 and MR-T2 image fused results of different fusion methods.

Table 1: The objective evaluation and running time for CT and MR image fused results of all methods.

	Q_0	Q_W	Q_E	$Q_{AB/F}$	MI
NSCT [1]	0.5960	0.7511	0.5707	0.5857	4.6665
NSCT [6]	0.5958	0.7554	0.5793	0.5892	4.6711
JSR [12]	0.6493	0.8148	0.6296	0.5838	3.6120
SR + NSCT [15]	0.6611	0.8477	0.6249	0.6447	4.0421
SR + NSCT [18]	0.6527	0.8161	0.5572	0.5866	3.6371
SR + SM	0.6566	0.8466	0.6992	0.6630	4.5467
SR + EM	0.6643	0.8355	0.6919	0.6477	4.2687
SR + SEM	**0.6679**	**0.8477**	**0.7043**	**0.6677**	**4.6721**

In all ratings, we can see that SR + SEM outperform other approaches. In addition, the suggested methods' effects are superior to those of other methods.

Fusion of CT and PET images in 3.3. As seen in Figure 3, the third experiment used 12 CT and PET picture pairs to measure the efficiency of these processes.Figure 7 depicts two sets of findings. NSCT and NSCT provide the better performance in terms of energy detail, allowing the fused images to collect both more spatial information in CT images and functional information contents in PET images. Doctors, on the other hand, ought to see the role of bone and tumor in clinical applications to assess anatomy and help in diagnosis. In Figures 7(r), 7(s), and 7, the findings fused by SR + SEMcontain more accurate details and higher contrast without information distortion, allowing one to easily see the shape of the kidney (t). Figure 7(b) shows nasopharyngeal carcinoma, and we can easily locate

International Journal of Multidisciplinary Engineering in Current Research
Volume 6, Issue 9, September 2021, http://ijmec.com/

it in Figure 7 SR+NSCT[15], SR + SM, and SR + SEM using the results fused by the proposed procedure, which are useful for viewing tumor behavior and helping physicians to better grasp the impact of cancer care. Table 3 lists the average scores of quantitative evaluationmetrics for 12CT and PET fused outcomes, with the "big" values indicating the maximum values. In any score, the SR + SEM outperform the other approaches. It demonstrates that this strategy is adaptable and secure.

The Time Complexity Analysis (3.4). To achieve 3D medical image fusion and reconstruction, a large number of CT/PET and MR/PET image slices must first be fused [37, 38].

As a result, a faster and more powerful image fusion algorithm is needed.As seen in Figure 8, we keep track of the total time spent by various approaches for 36 separate medical picture pairs. Multiscale methods such as NSCT [1] and NSCT are clearly faster, while SR-based approaches (JSR SR+NSCT and SR +NSCT take much longer. In comparison, the time taken by SR + SM, SR + EM, and SR + SEM is around 1/50 of the time taken by the SR-based solution. We may conclude from the aforementioned study and debate that SR + SEM outperforms all others in the field of medical picture fusion. Our approaches are easier for doctors to localize irregular masses and tumors in patients because they provide more original detail from source pictures and more local structure information.

4. Conclusion

A new medical image fusion method based on SR and feature extraction is proposed in this article.When opposed to traditional SR-based fusion approaches, there are at least three significant advances. To begin, we propose three decision maps to boost the accuracy of SR-based image fusion methods in extracting the source images' structure and energy features. This technique will help keep as many of the initial data from the source photos as possible.Second, we incorporate the decisionmap into the SRbasedmethods to speed up the algorithm. The suggested solution requires just 1/50 of the time that the conventional SR process does to achieve picture fusion. Third, using source picture structure and energy details in the decision chart greatly improves the accuracy of the fused data. The findings of the tests show that the proposed fusion process will produce greater results in both subjective and quantitative ways than traditional fusion approaches.

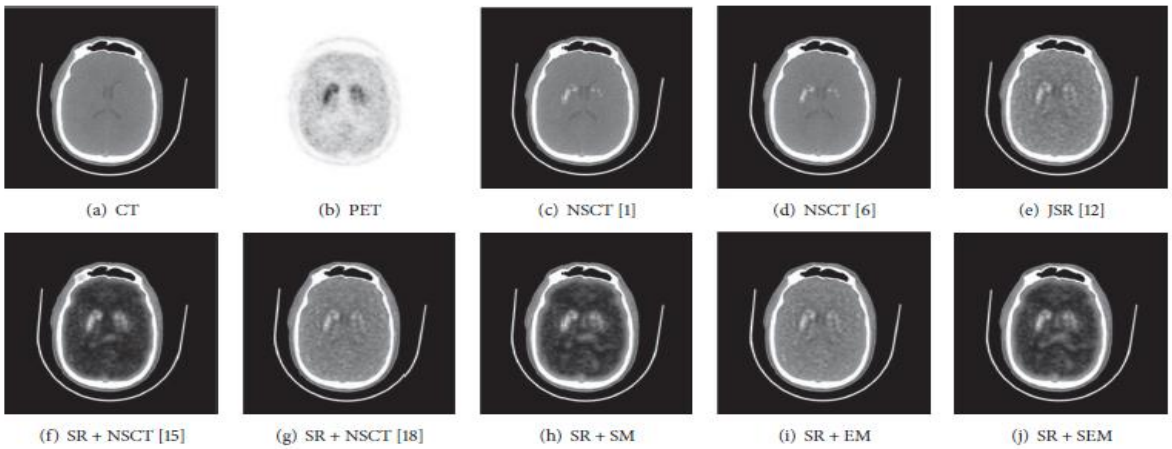

International Journal of Multidisciplinary Engineering in Current Research
Volume 6, Issue 9, September 2021, http://ijmec.com/

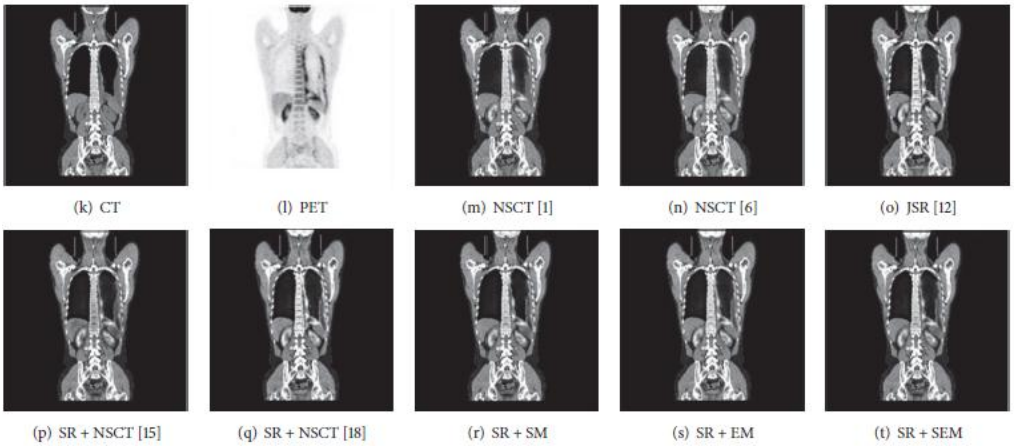

Figure 7: The CT and PET image fused results of different fusion methods.

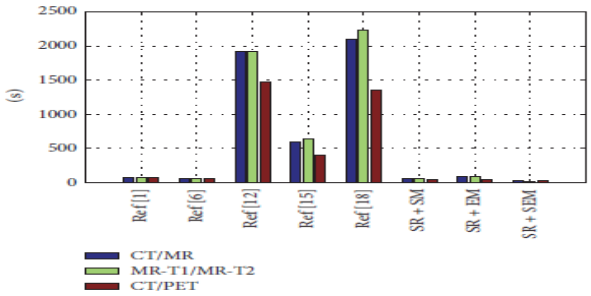

Figure 8: The time consuming of different fusion methods.

References

[1] P. S. Gomathi and B. Kalaavathi, "Multimodal medical imagefusion in non-subsampled contourlet transform domain," Circuits& Systems, vol. 7, no. 8, pp. 1598–1610, 2016.

[2] M. D. C. Vald´esHern´andez, K. J. Ferguson, F.M. Chappell, andJ. M. Wardlaw, "New multispectral MRI data fusion technique for white matter lesion segmentation: method and comparisonwith thresholding in FLAIR images," European Radiology, vol.20, no. 7, pp. 1684–1691, 2010.

[3] Z. Liu, H. Yin, Y. Chai, and S. X. Yang, "A novel approach formultimodal medical image fusion," Expert Systems with Applications,vol. 41, no. 16, pp. 7425–7435, 2014.

[4] Y. Yang, S.Tong, S. Huang, andP.Lin, "Log-Gabor energy basedmultimodal medical image fusion in NSCT domain," Computationaland Mathematical Methods in Medicine, vol. 2014,Article ID 835481, 12 pages, 2014.

[5] V. D. Calhoun and T. Adali, "Feature-based fusion of medicalimaging data," IEEE Transactions on Information Technology inBiomedicine, vol. 13, no. 5, pp. 711–720, 2009.

[6] P. Ganasala and V. Kumar, "CT and MR image fusion schemein nonsubsampledcontourlet transform domain," Journal ofDigital Imaging, vol. 27, no. 3, pp. 407–418, 2014.

[7] R. Shen, I. Cheng, and A. Basu, "Cross-scale coefficient selectionfor volumetric medical image fusion," IEEE Transactionson Biomedical Engineering, vol. 60, no. 4, pp. 1069–1079, 2013.

[8] Z. Wang and Y. Ma, "Medical image fusion using m-PCNN,"Information Fusion, vol. 9, no. 2, pp. 176–185, 2008.

[9] G. Bhatnagar, Q. M. Jonathan Wu, and Z. Liu, "Human visualsystem inspiredmulti-modalmedical image fusion framework,"Expert Systems with Applications, vol. 40, no. 5, pp. 1708–1720,2013.

[10] L. Yang, B. L. Guo, and W. Ni, "Multimodality medical imagefusion based on multiscale geometric analysis of contourlettransform," Neurocomputing, vol. 72, no. 1-3, pp. 203–211, 2008.

[11] M. Kim, D. K. Han, and H. Ko, "Joint patch clustering-baseddictionary learning for multimodal image fusion," InformationFusion, vol. 27, pp. 198–214, 2016.

[12] Y. Yao, P. Guo, X. Xin, and Z. Jiang, "Image fusion by hierarchicaljoint sparse representation," Cognitive Computation, vol. 6,no. 3, pp. 281–292, 2014.

[13] T. Guha and R. K. Ward, "Learning sparse representationsfor human action recognition," IEEE Transactions on PatternAnalysis and Machine Intelligence, vol. 34, no. 8, pp. 1576–1588,2012.

[14] S. T. Li, H. T. Yin, and L. Y. Fang, "Group-sparse representationwith dictionary learning for medical image denoising andfusion," IEEE Transactions on Biomedical Engineering, vol. 59,no. 12, pp. 3450–3459, 2012.

[15] Y. Liu, S. Liu, and Z. F. Wang, "Medical image fusion by combiningnonsubsampledcontourlet transform and sparse representation,"in Pattern Recognition, vol. 484 of Communicationsin Computer and Information Science, pp. 372–381, Springer,Berlin, Germany, 2014.

[16] H. Yin, S. Li, and L. Fang, "Simultaneous image fusionand super-resolution using sparse representation," InformationFusion, vol. 14, no. 3, pp. 229–240, 2013.

[17] C. M. Falco, X. Jiang, F. Yin, W. Gao, and Z. Song, "Imagefusion based on group sparse representation," in Proceedings ofthe Eighth International Conference on Digital Image Processing(ICDIP '16), Chengu, China, August 2016
.
[18] J. Wang, J. Peng, X. Feng, G. He, J. Wu, and K. Yan, "Imagefusion with nonsubsampledcontourlet transform and sparserepresentation," Journal of Electronic Imaging, vol. 22, no. 4,Article ID 043019, 2013.

[19] Q.H. Zhang, Y. L. Fu, H. F. Li, and J. Zou, "Dictionary learningmethod for joint sparse representation-based image fusion,"Optical Engineering, vol. 52, no. 5, pp. 532–543, 2013.

[20] B. Yang and S. Li, "Visual attention guided image fusion withsparse representation," Optik, vol. 125, no. 17, pp. 4881–4888,2014.